Available online at www.sciencedirect.com
ScienceDirect
Trans. Nonferrous Met. Soc. China 31(2021) 1262−1275
Transactions of Nonferrous Metals Society of China
www.tnmsc.cn

Tribological properties improvement of conventionally-cast Al−8.5Fe−1.3V−1.7Si alloy by multi-pass friction stir processing

Z. NOURI, R. TAGHIABADI

Department of Materials Science and Metallurgy, Imam Khomeini International University, Qazvin, Iran

Received 25 May 2020; accepted 26 November 2020

Abstract: The effect of multi-pass friction stir processing (FSP) on the tribological properties of conventionally-cast Al−8.5Fe−1.3V−1.7Si (FVS0812) alloy was investigated. The pin-on-disk dry sliding wear tests were conducted at room temperature under the applied pressures of 0.25, 0.50, and 0.75 MPa. The results showed that FSP substantially refined and improved the distribution of coarse θ-$Al_{13}Fe_4$ platelets and α-$Al_{12}(Fe,V)_3Si$ intermetallics in the microstructure of alloys and eliminated the intermetallic-related defects. Consequently, the mechanical properties of the alloys, especially their ductility, were improved, which enhanced the stability of the protective tribolayer formed on their worn surfaces. According to the wear test results, the FSPed samples showed improved tribological properties especially at the higher applied pressures. For instance, at the applied pressure of 0.75 MPa, the wear rate and average friction coefficient of four-pass FSPed sample were lower than those of the base as-cast sample by 97% and 52%, respectively. SEM examination of the worn surfaces and wear debris also demonstrated that the wear mechanism changed from severe delamination/abrasion and microcracking of the tribolayer in the as-cast samples to mild delamination/abrasion and minor plastic wear in the FSPed samples.

Key words: friction stir processing; Al−8.5Fe−1.3V−1.7Si (FVS0812) alloy; intermetallic; tribology

1 Introduction

Al−8.5Fe−1.3V−1.7Si (FVS0812), Al−12.4Fe−1.15V−2.3Si (FVS1212) and Al−5.5Fe−0.5V−1.1Si (FVS0512) are the well-known heat-resistant Al−Fe−V−Si alloys, which due to their high ductility, high fracture toughness, high fatigue resistance at room temperature, and high heat resistance at high temperatures (up to 400 °C) have been employed in industrial applications such as automotive, aerospace, and aviation industries [1,2].

The improved high temperature properties of these alloys stem from the presence of intermetallics rich in transition metals such as Fe and V in their microstructure which are highly stable at high-temperature services and serve as strengthening precipitates provided that their size and distribution within matrix are optimized [3,4]. Therefore, these alloys are usually fabricated by rapid solidification processing (RSP) techniques such as melt spinning, spray deposition, and gas/water atomizing followed by subsequent consolidation techniques [3−10] such as hot extrusion, hot pressing/hot extrusion, mechanical alloying/hot pressing, mechanical alloying/spark plasma sintering, selective laser melting, and electron beam melting.

The high solidification rate applied during RSP (typically 10^2−10^7 K/s), on one hand, leads to the formation of ultrafine grains and appropriate precipitates such as α-$Al_{12}(Fe,V)_2Si$ and extends the solid solution by solute trapping and, on the other hand, prevents the formation of inappropriate intermetallic compounds such as needle-like θ-$Al_{13}Fe_4$

Corresponding author: R. TAGHIABADI, E-mail: taghiabadi@ikiu.ac.ir
DOI: 10.1016/S1003-6326(21)65576-0

in the microstructure improving high-temperature properties [11,12]. However, the RSP techniques are generally time-consuming, need special equipment, and suffer from high capital/operational costs [13−15]. Moreover, the large surface-to-volume ratio of rapidly-solidified products such as ribbons and powders is likely to increase the amount of entrained oxide inclusions. In addition, increasing the temperature of components during the supplementary fabrication stages such as extrusion can alter the microstructure and mechanical properties [13]. Therefore, many attempts have been conducted to develop the economical methods capable of improving the mechanical properties of conventionally-cast Al−Fe−V−Si alloys, the most important of which are chemical modification and thermo-mechanical processing.

LIU et al [15] studied the effect of Ce modification on the microstructure and mechanical properties of Al−5.5Fe−1.1V−0.6Si alloy solidified under the near rapid solidification rate (~30 °C/s). They found that Ce addition modified the primary $Al_{13}(Fe,V)_3Si$ compounds and improved the mechanical properties so that the ultimate tensile strength and elongation of the alloy increased by 76% and 73%, respectively. The positive effect of Mg and Ni−Mg addition on morphology of primary θ-$Al_{13}Fe_4$ needles in the microstructure of conventionally-cast Al−8.3Fe−0.8V−Si alloys was demonstrated by SAHOO et al [16,17]. This was attributed to the interfacial segregation and/or absorption of Mg and Ni atoms into the lattice of θ-phase. In another work, SAHOO et al [18] showed the positive influence of Mg and/or Ni−Mg addition on the wear resistance and friction behavior of conventionally-cast Al−8.3Fe−0.8Fe−0.9Si alloy. The combined effect of Ni−Mg modification and hot rolling on the tensile strength of Al−8Fe−1V−1Si alloy was also investigated by SAHOO and PATHAK [19]. The results showed that the tensile strength of modified and hot-rolled sample was higher than that of un-modified and modified samples by 240% and 20%, respectively.

FSP is another thermo-mechanical processing method which is widely used for developing alloys with modified microstructures and improved mechanical properties. In this process, a rotating wear-resistant tool consisting of a shoulder and a pin is plunged into the alloy surface until its shoulder comes in contact with the surface. Then, the tool moves along the desired direction to process the alloy (Fig. 1) [20,21]. Despite the proven effect of FSP on improving tribological properties of different Al-based alloys and composites, little attention has been paid so far to its effect on the tribology of Al−Fe−X alloy systems. In a recent study, FEKRI SOUSTANI et al [22] investigated the effect of FSP on the tribological properties of conventionally-cast Al−7Fe−5Ni alloy and showed that, due to the effective refinement of coarse Al_9FeNi intermetallics, elimination of casting defects, and grain refinement, FSP considerably enhanced the wear resistance and friction behavior of Al−7Fe−5Ni alloy.

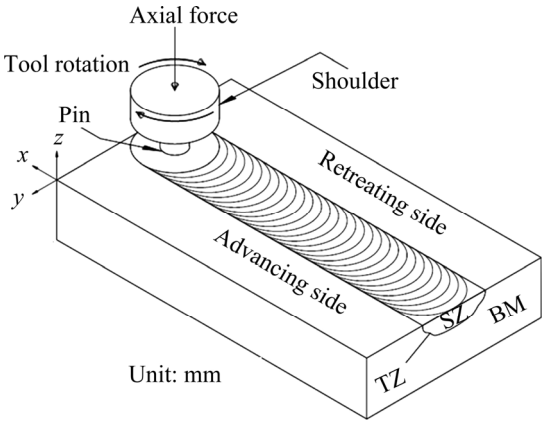

Fig. 1 Schematic diagram of friction stir processing

Therefore, this study was conducted with the aim of investigating the capability of the FSP process, as an efficient, economic, and simple-to-use alternative to the other modification techniques, in improving the tribological properties of the conventionally cast Al−8.5Fe−1.3V−1.7Si (FVS0812) alloy.

2 Experimental

The chemical composition of Al−8.5Fe−1.3V−1.7Si used in the present study is given in Table 1. The alloy was produced by melting high purity Al (99.9 wt.%), Al−20Fe, Al−30Si, and Al−15V master alloys in an induction furnace (380 V, 37 A, and 10 kHz) under the protection of high purity Ar atmosphere (99.999 wt.%). When the melting process was completed and a homogenized composition was achieved, the melt was degassed by dry hexachloroethane (1 wt.% of alloy) to lower the hydrogen content. Then, the melt temperature

increased up to 850 °C, the surface dross was removed, and the melt was gently stirred by a graphite rod before being poured into a preheated cast-iron mold (250 °C) to obtain slabs with dimensions of 150 mm × 100 mm × 10 mm. The average cooling rate of the mold was 4.8 °C/s.

Table 1 Chemical composition of FVS0812 alloy (wt.%)

Fe	Si	V	Other	Al.
8.41±0.03	1.73±0.03	1.34±0.02	<0.1	Bla.

The obtained slabs were subjected to FSP using a plain cylindrical tool made of an AISI H13 tool steel (Fig. 2(a)) with the hardness of HRC (58±2). The FSP was conducted by the optimized parameters (rotation speed of 1600 r/min and traverse speed of 12 mm/min) [23] for one, two, and four passes. The tool plunge depth was set to 0.3 mm. The obtained FSPed samples were coded as *n*P-FSP, where *n* denotes the number of applied passes. An Avio infrared camera with an accuracy of ±2 °C was employed to measure the average peak temperature at the interface of the pin tool and the substrate.

For tensile testing and dry sliding wear tests, the samples were cut by wire cutting tool from the FSPed zone along the processing direction (Fig. 2(b)). The tensile tests were performed using a Zwick/Roell-Z100 universal tensile testing machine at the crosshead speed of 0.1 mm/min. The average tensile properties of three specimens were reported. The Vickers microhardness of the samples was measured by a Gnehm-Härteprüfer FM100 microhardness tester with the load of 500 g for 15 s on the transverse cross-section of the FSPed zone perpendicular to the tool traverse direction. The average of six indentation tests was reported.

Room-temperature pin-on-disk wear tests were conducted by a TR−20 DUCOM testing machine in accordance with ASTM G 99–90. The wear tests were conducted at the applied pressures of 0.25, 0.5, and 0.75 MPa, at the constant sliding speed of 0.13 m/s for a sliding distance of 1000 m with the relative humidity (RH) controlled at (56±5)%. The geometry and dimensions of the pins are shown in Fig. 2(b). In order to obtain a flat conformal contact between the pin and the disk, the bottoms of all the pins were preliminarily run-in against an SiC abrasive paper (P1500) rigidly fixed on the disc surface under the same experimental conditions for

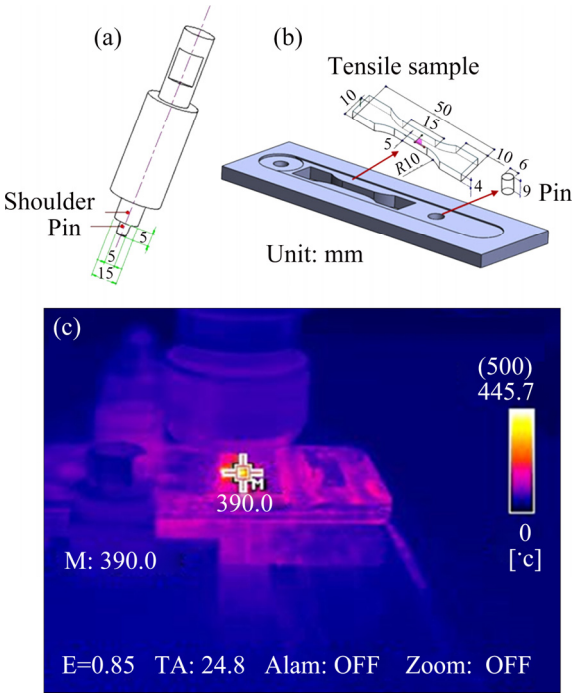

Fig. 2 Geometry and dimensions of FSP tool (a), tensile and wear test samples and sampling position (b), and typical infrared thermography image illustrating maximum surface temperature during FSP of 1P-FSP sample (c)

10 min. The disk material was made of hardened AISI 52100 steel with the hardness of HRC (60±2) to make the pin wear the controlling factor.

Samples for metallographic examinations, taken from the FSPed area normal to the processing direction, were prepared by standard metallographic procedures and etched by the Keller's reagent (1 mL HF, 1.5 mL HCl, 2.5 mL HNO_3, and 95 mL distilled water) for 10 s. Microstructural observations were performed using a Tescan-Vega scanning electron microscope (SEM). The microscopic examination of the worn surfaces, wear debris, and subsurface regions was also performed by SEM. The porosity of the samples was calculated by the Archimedes' principle as described comprehensively by TAYLOR et al [24].

3 Results and discussion

3.1 Microstructural characterization

The as-cast microstructure of the base alloy (Fig. 3) shows that light gray needle-like and medium gray irregular-shaped particles are distributed within the dark gray α-Al matrix. According to the EDS microanalysis results shown

in Table 2 and in consistent with the previous findings [16,25,26], light and medium gray phases are θ-$Al_{13}Fe_4$ and α-$Al_{12}(Fe,V)_3Si$, respectively. The presence of micropores is also evident in the microstructure. Due to degassing the melt, the majority of these micropores are likely shrinkage-driven pores that have been formed as a result of blocking the liquid feeding paths by the primary θ-$Al_{13}Fe_4$ needles. However, the rejection of H-atoms into the remaining liquid ahead of solidification front, especially in the presence of elements like Fe which reduces the H solubility in molten Al [27], is likely to promote the formation of mixed-type (gas and shrinkage) micropores.

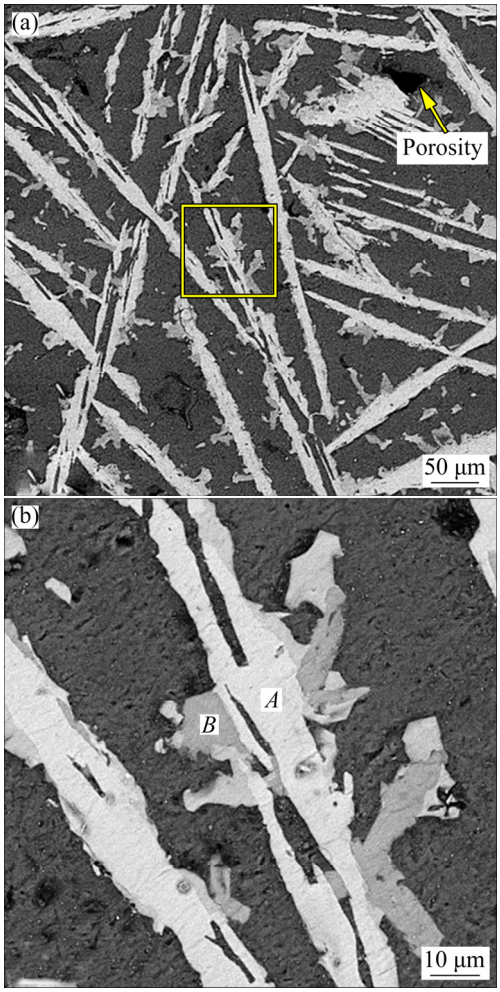

Fig. 3 SEM images of base FVS0812 alloy (a) and enlarged view (b) of boxed area in (a)

Table 2 EDS analysis of marked phases shown in Fig. 3(b) (wt.%)

Phase	Al	Fe	V	Si
θ-$Al_{13}Fe_4$ (Point *A*)	19.43	80.57	−	−
α-$Al_{12}(Fe,V)_3Si$ (Point *B*)	15.89	82.62	1.49	−

The positive effect of FSP on refinement and densification of the microstructure of FVS0812 alloy is observed in Fig. 4. Figure 4(a) shows the overall microstructure of three zones in the 1P-FSP sample: stir zone (SZ), thermomechanically affected zone (TMAZ), and unaffected base metal

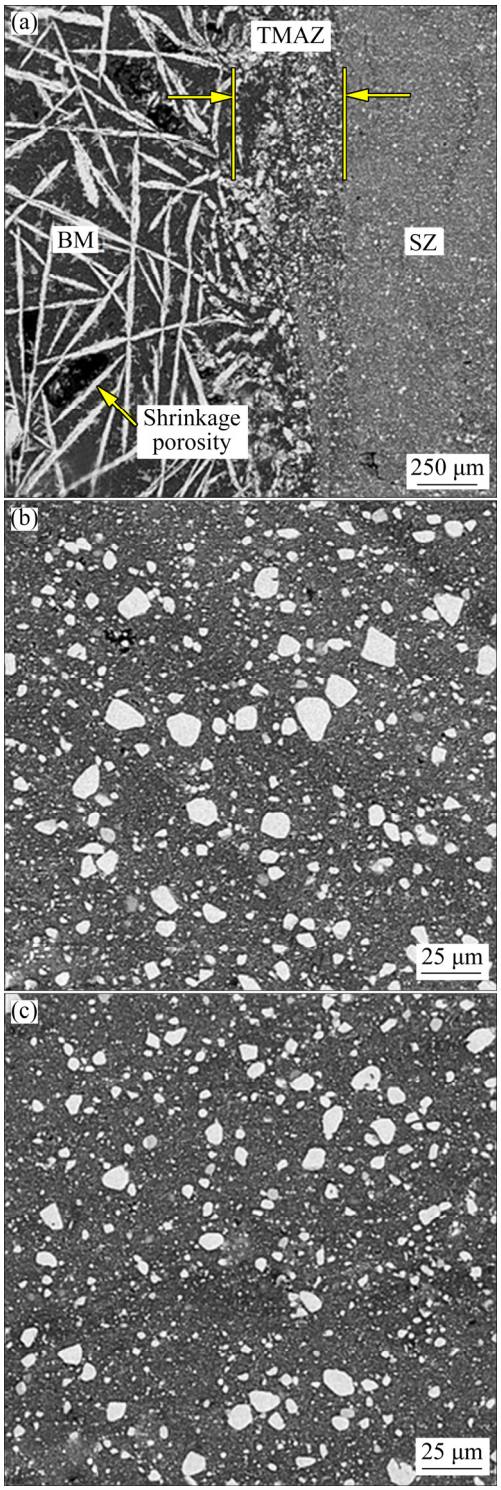

Fig. 4 SEM images showing microstructure of 1P-FSP sample at boundary between SZ and unaffected BM (a), SZ of 1P-FSP (b), and SZ of 4P-FSP (c) samples

(BM). The magnified images showing the SZ microstructures of 1P-FSP and 4P-FSP samples are also shown in Figs. 4(b) and (c), respectively. As seen, due to the simultaneous effect of frictional heating (Fig. 2(c)) and severe plastic deformation, the SZ material has been aggressively deformed, which resulted in breakage and uniform distribution of coarse intermetallic particles and forging of the micropores. According to the image analysis results (Table 3), compared to the base sample, the average size of intermetallic particles has decreased by almost 100% in FSPed samples. Moreover, the volume fraction of porosities, measured by the Archimedes' method, has reduced from 2.83% in the base alloy to 0.54%, 0.51%, and 0.47% in 1P-, 2P-, and 4P-FSP samples, respectively. By comparing the SZ microstructures (Figs. 4(b, c)) and image analysis results (Table 3), it seems that applying the second and forth passes of FSP results in homogenization and densification of microstructures rather than refining the existing intermetallic particles. This is probably due to the fact that, compared to the large plate-like particles, the small equiaxed intermetallics have experienced lower levels of deformation torques.

Table 3 Image analysis results of base and FSPed samples

Sample	Average size of Fe-rich intermetallics/μm		Porosity/ vol.%
	Needle-like	Polyhedral	
Base	128.31±23.03	32.91±10.27	2.83
1P-FSP	−	0.56±0.14	0.54
2P-FSP	−	0.50±0.18	0.51
4P-FSP	−	0.43±0.09	0.47

The effect of FSP on the mechanical properties of FVS0812 alloy is shown in Table 4. As seen, applying the first pass of FSP has substantially improved the mechanical properties. For instance, the tensile strength, fracture strain, and hardness of 1P-FSP sample are higher than those of the base sample by about 1000%, 930%, and 63%, respectively. This can be attributed to the severe breakage of needle-like θ-$Al_{13}Fe_4$ intermetallics and the elimination of θ-related defects in the microstructure. The needle-like intermetallics, due to their high aspect ratio which significantly restricts the gliding of dislocations, act as stress risers in the matrix [28]. However, regarding their brittle nature arising from their complex crystal structure [29] and their weak faceted-type interfaces arising from their high melting entropy [30], these particles are easily broken under high accumulated stresses leading to the premature microcracking and fracture of the alloy. Moreover, the plate-like morphology of θ particles increases their potential in impeding the liquid metal flow [30], thereby increases the formation probability of shrinkage micropores in the microstructure (Figs. 3 and 4(a) and Table 3). Micropores are detrimental defects that reduce the effective load-bearing cross-section and act as stress risers in the microstructure deteriorating the mechanical properties and castings reliability [31].

Table 4 Effect of multi-pass FSP on mechanical properties of FVS0812 alloy

Sample	Tensile strength/MPa	Fracture strain/%	$HV_{0.5}$
Base	25.6±6.5	0.23±0.11	80.2±7.3
1P-FSP	285.4±15.4	2.37±0.22	130.3±12.2
2P-FSP	318.1±16.8	4.60±0.50	147.5±7.4
4P-FSP	336.9±10.9	7.91±0.12	160.1±5.1

Figure 5 depicts the fracture surface of the base, 1P-FSP and 4P-FSP alloys. The presence of coarse and brittle θ-$Al_{13}Fe_4$ needles, θ-phase-related shrinkage micropores, and brittle α-$Al_{12}(Fe,V)_3Si$ particles on the fracture surface of the base (Fig. 5(a)) indicates their critical role in low-energy brittle fracture of this sample.

Therefore, decreasing the size of intermetallics in the FSPed samples is likely to reduce the amplitude of stress concentrated on them, enhance their resistance against microcracking/decohesion, and increase their potential in Orowan strengthening [32]. FSP also densifies the microstructure and leads to the formation of fine dynamically-recrystallized grains which play a significant role in improving hardness/mechanical strength by the grain boundary strengthening. Increasing the number of dislocations in the SZ [22] and improving the bonding quality of particles/ matrix interface [33] are the other FSP-related factors enhancing the mechanical properties.

According to Table 4, applying multiple passes of FSP relatively increases the tensile strength and

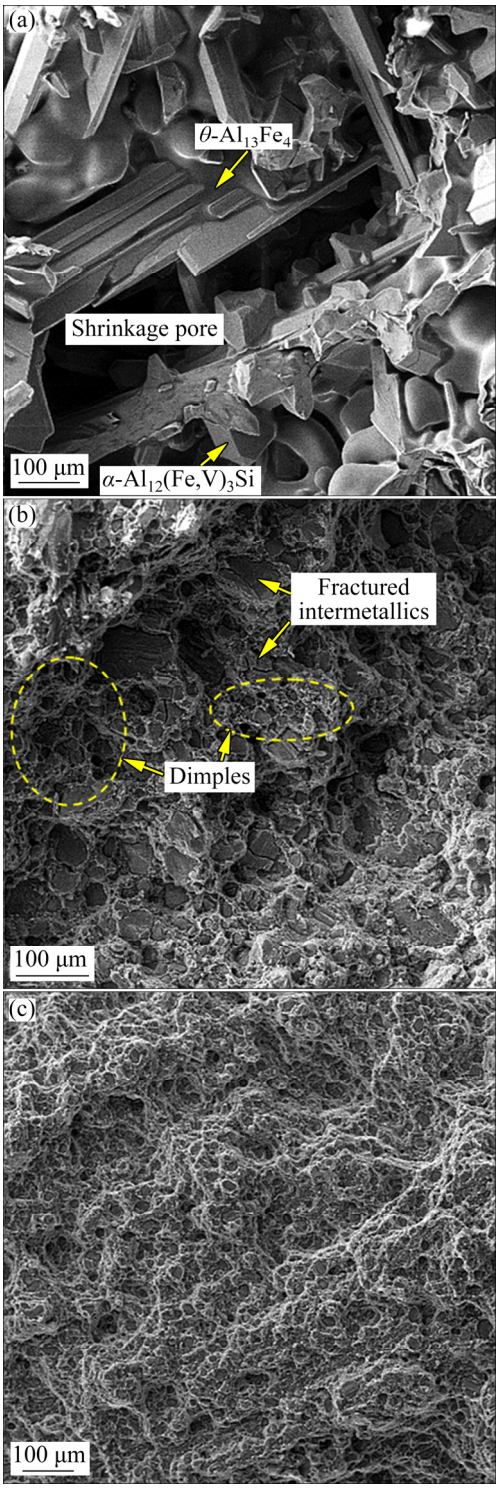

Fig. 5 SEM images showing fracture surface of base (a), 1P-FSP (b), and 4P-FSP (c) samples

hardness of 1P-FSP sample, while substantially improves its fracture strain. For instance, the tensile strength and hardness of 4P-FSP sample are higher than those of 1P-FSP by 18% and 23%, respectively, but its fracture strain increases by about 230%. The relative enhancement of tensile strength and hardness with the increasing number of FSP passes can be mainly attributed to the size reduction of intermetallic dispersoids and higher strength of the particles/matrix bonding. The former is likely to increase the fraction of the particles capable of providing Orowan strengthening while the latter increases the load-transfer capability between the matrix and the particles. The substantial improvement of the alloy ductility can be also explained by the significant improvement of particles distribution and reduction of casting defects as it is evident from Fig. 4. This is also confirmed by the fractography investigation results.

Figure 5(b) shows the fracture surface of 1P-FSP sample. As seen, in agreement with the microstructural characterization results (Fig. 4 and Table 3) and mechanical properties (Table 4), applying the first pass of FSP has considerably refined the brittle intermetallic compounds in a way that a more ductile fracture appearance comprising of dimpled areas and brittle-fractured intermetallic particles is evident (Fig. 5(b)). Figure 5(c) shows the fracture surface of 4P-FSP sample. The extensive refinement/homogeneous distribution of Fe-rich intermetallic compounds, the elimination of large micropores, and extensive formation of dimples are the most prominent features of the fracture surface of 4P-FSP sample which are responsible for its improved tensile properties.

3.2 Tribological properties

The effect of multi-pass FSP on the wear behavior of FVS0812 alloy at different applied pressures of 0.25, 0.50, and 0.75 MPa is shown in Fig. 6. As it is evident, applying FSP decreases the

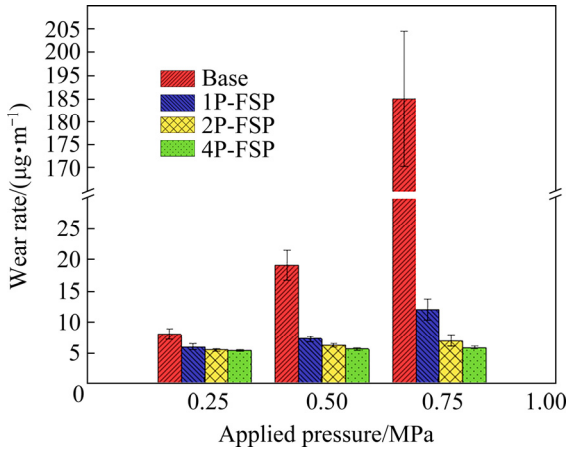

Fig. 6 Wear rate variation of base and multi-pass FSPed samples against applied pressure

alloy's wear especially at the higher applied pressures. For instance, at the applied pressures of 0.25 and 0.75 MPa, the wear rate of 1P-FSP samples is lower than that of the base sample by 25% and 93%, respectively. It is also evident from the wear results that increasing the number of FSP passes improves the wear resistance of the alloy so that at the applied pressure of 0.75 MPa, the wear rates of 2P-FSP and 4P-FSP samples are lower than that of 1P-FSP by 42% and 50%, respectively.

Figure 7 shows the worn surface of the base sample tested at the applied pressures of 0.25 and 0.75 MPa. The EDS analysis results (Fig. 8) confirm the formation of oxide-rich tribolayer on the worn surface of the base sample. This indicates the oxidative wear mechanism that includes generation, oxidation, sintering, and compaction of fine loose wear particles.

The formation of the delaminated craters on the worn surfaces indicates the delamination wear as another important wear mechanism. However, the formation of shallow delaminated craters and tiny abrasion tracks on the worn surface of the base sample worn at the applied pressure of 0.25 MPa suggest that its wear is in the mild wear regime. It seems that the substantial increase of substrate's hardness (Table 4) mediated by the presence of high volume fractions of hard Fe-rich intermetallics reduces its deformation against the friction-induced surface strains (Fig. 9(a)), thereby improving the tribolayer stability on the worn surface.

Figures 7(b) and (c) show the worn surface of the base sample tested at the applied pressure of 0.75 MPa. In agreement with the wear results (Fig. 6), the severe delamination/microcracking of the tribolayer and generation of the large plate-like/lumpy wear particles (Fig. 7(d)) are the indications of severe wear in this sample.

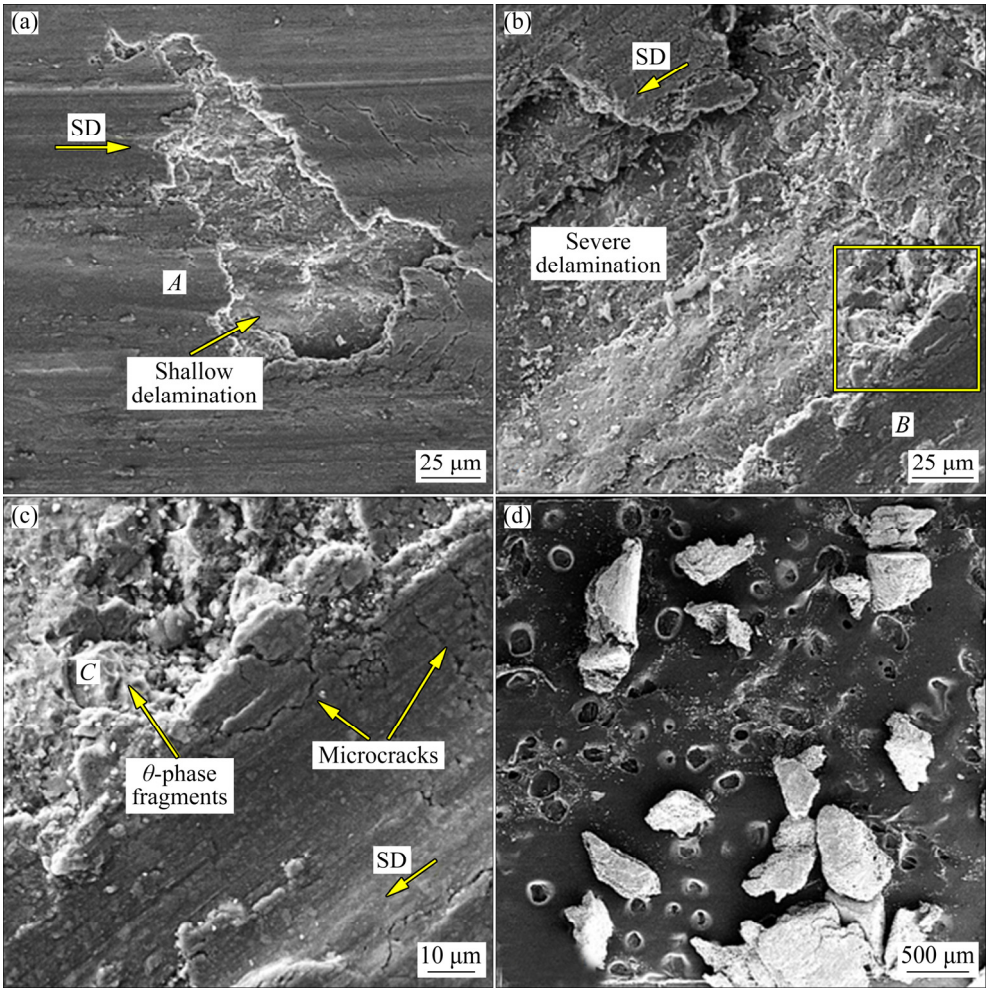

Fig. 7 SEM images showing worn surfaces morphology of base at applied pressures of 0.25 MPa (a) and 0.75 MPa (b), respectively, enlarged view (c) of boxed area in (b), wear debris morphology (d) of base collected after wear test at applied pressure of 0.75 MPa (SD stands for sliding direction)

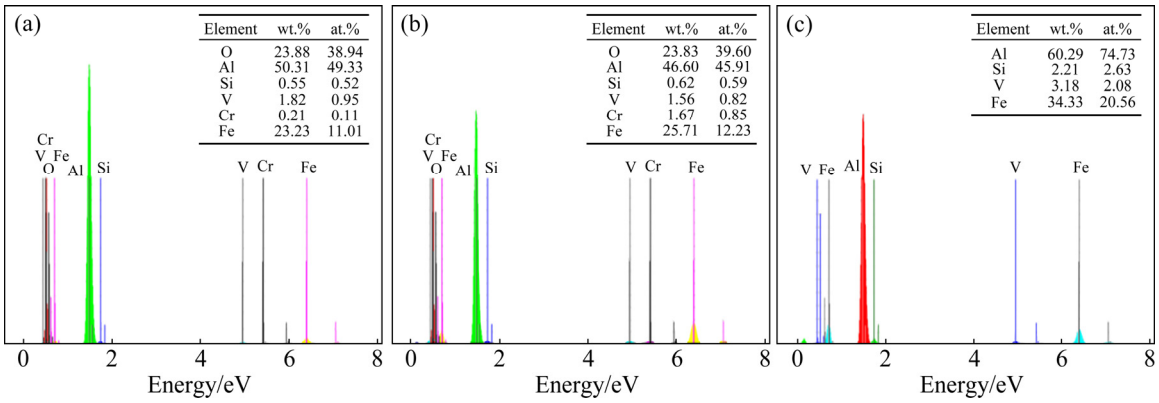

Fig. 8 EDS analyses of marked points shown in Fig. 7: (a) Point *A*; (b) Point *B*; (c) Point *C*

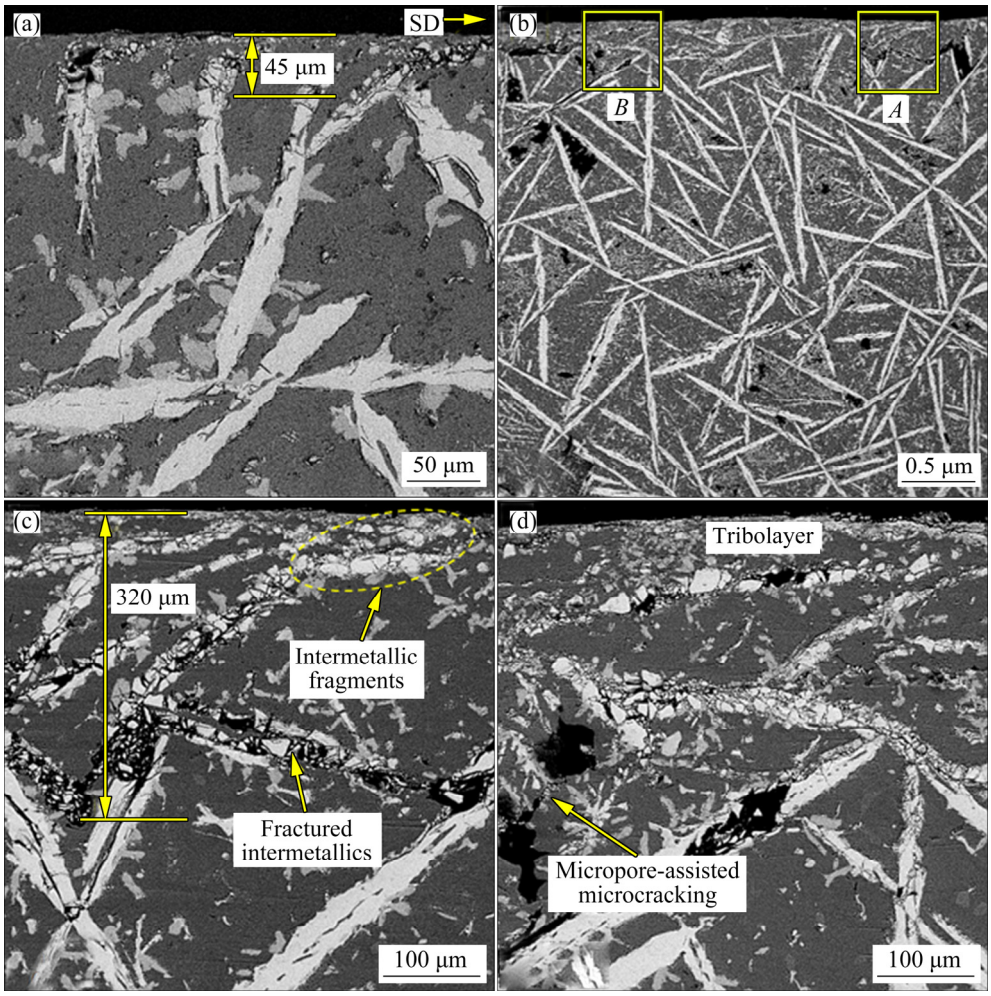

Fig. 9 Worn subsurface microstructures of base at applied pressures of 0.25 MPa (a) and 0.75 MPa (b), enlarged views of zones *A* (c) and *B* (d) shown in (b), respectively

Figure 9(b) depicts the worn subsurface microstructure of the base sample tested at the applied pressure of 0.75 MPa. The enlarged views of zones *A* and *B* shown in Fig. 9(b) are shown in Figs. 9(c) and (d), respectively. As seen, at the applied pressure of 0.75 MPa, the substrate has experienced substantial deformation (Fig. 9(c)), about eight times of the sample tested at the applied pressure of 0.25 MPa (Fig. 9(a)), and the existing intermetallics especially the coarse plate-like θ-phases have been severely broken. The breakage of θ-particles and formation of θ-fragments with

low aspect ratio not only decrease their potential in impeding dislocation motion, but also promote the formation of subsurface microcracks that are gradually propagated towards the surface (Fig. 9(c)) weakening the substrate. The gradual incorporation of θ-fragments into the tribolayer (Fig. 9(c)) also decreases its compactness/strength, thereby facilitating its removal from the surface (Figs. 7(b, c)). Moreover, the accumulation of hard intermetallic fragments between the mating surfaces may promote two- or three-body abrasive wear. The high concentration of Cr element in the tribolayer composition (Fig. 8(b)) indicates the abrasion of disk material by the pin. Therefore, the presence of coarse θ-platelets in the substrate although improves its hardness (Table 4), due to encouraging microcracking and defect formation (Figs. 9(c, d)), impairs its resistance against sliding-induced strains.

The worn surface morphologies of 1P-FSP and 4P-FSP samples tested at the applied pressures of 0.25 and 0.75 MPa are shown in Fig. 10. As seen, regardless of the applied pressure and the number of FSP passes, all the worn surfaces have been covered by protective oxide-rich tribolayers (Fig. 11) which have experienced minor damage. The morphology of the wear debris collected during the sliding wear of 1P-FSP and 4P-FSP samples at the applied pressure of 0.75 MPa is also shown in Fig. 12. As seen, in agreement with the wear results (Fig. 6) and worn surface morphology (Fig. 10), the wear debris is mainly composed of ultrafine equiaxed particles. Therefore, oxidative wear and mild delamination/abrasion of the oxide-rich tribolayer are suggested as the prominent wear mechanisms of multi-pass FSPed samples.

Figure 13 depicts the effect of multi-pass FSP on the worn subsurface microstructure of base

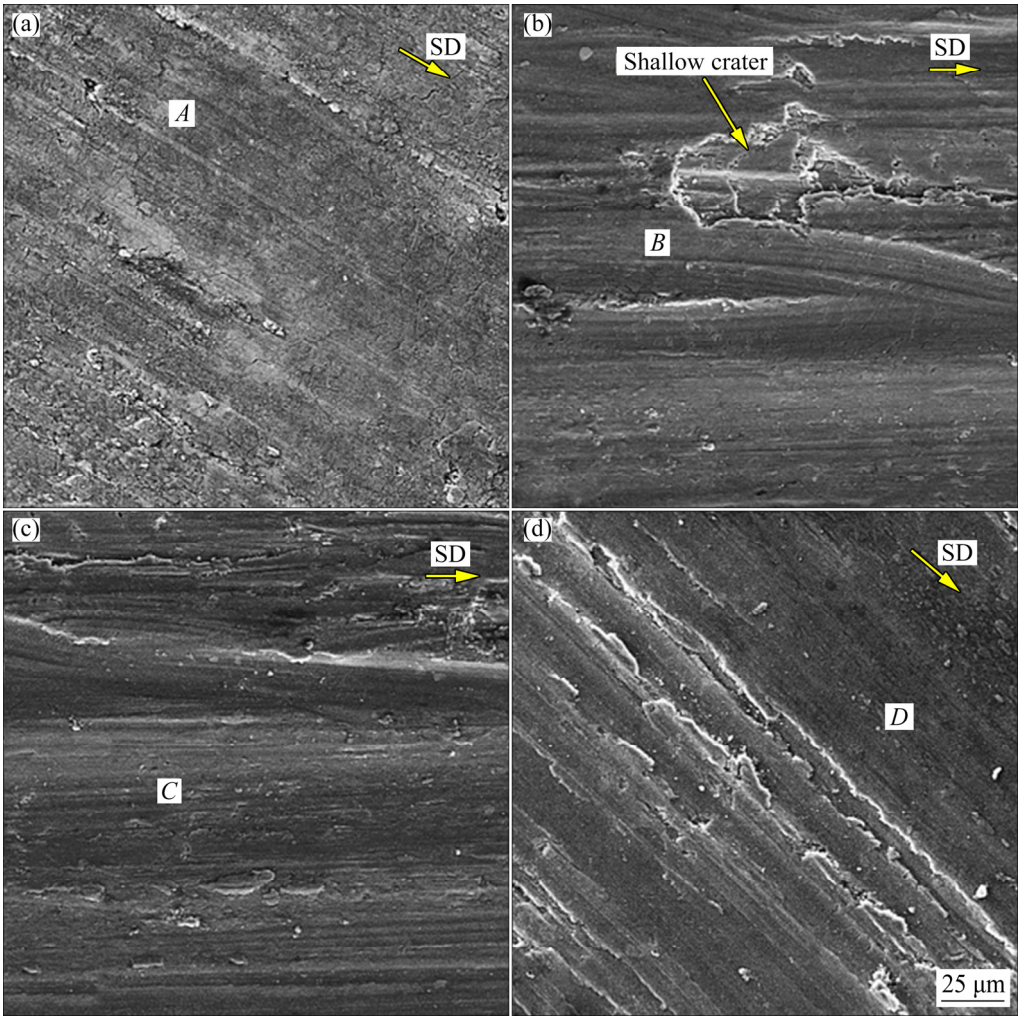

Fig. 10 SEM images showing worn surface morphologies of 1P-FSP (0.25 MPa) (a), 1P-FSP (0.75 MPa) (b), 4P-FSP (0.25 MPa) (c), and 4P-FSP (0.75 MPa) (d)

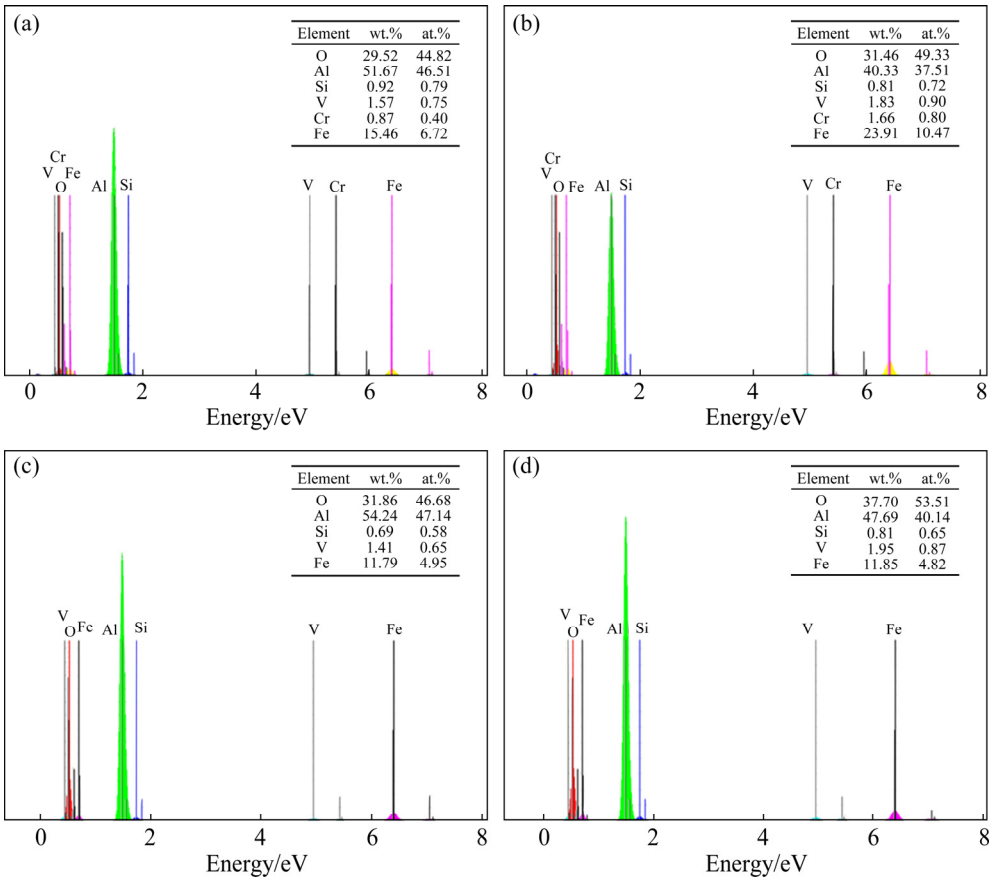

Fig. 11 EDS analyses of marked points shown in Fig. 10: (a) Point *A*; (b) Point *B*; (c) Point *C*; (d) Point *D*

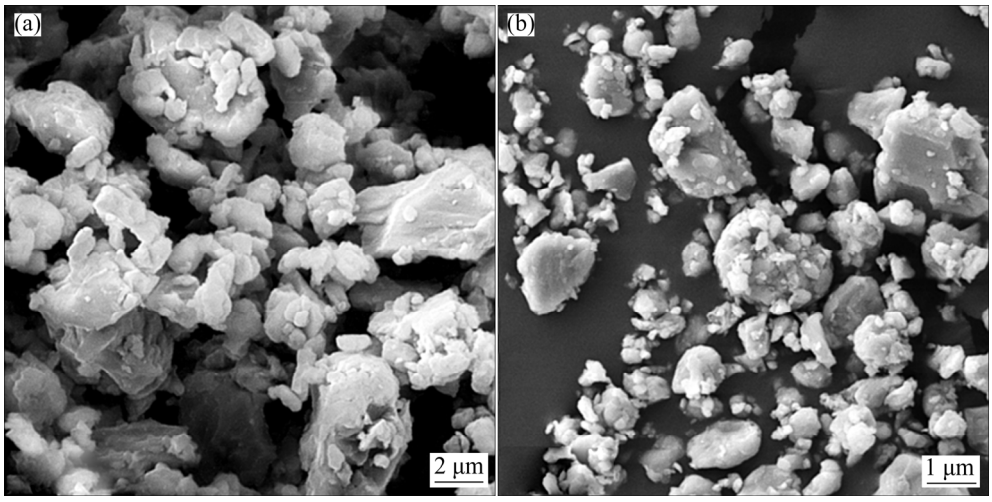

Fig. 12 SEM images showing wear debris morphology of 1P-FSP (a) and 4P-FSP (b) samples after sliding wear at applied pressure of 0.75 MPa

FVS0812 alloy tested at the applied pressure of 0.75 MPa. As seen, compared to the substrate microstructure of the base sample worn at a same applied pressure (Figs. 9(b−d)), particles fracture and/or severe microcracking are not observed in the substrate microstructure of FSPed samples. Moreover, the FSPed samples show minor plastic deformation in their substrate layers (Fig. 9(c)), and this is most likely the reason why their worn surfaces have been covered by protective stable tribolayers (Fig. 10). On this basis, the increased wear resistance of the FSPed samples, especially those subjected to the higher FSP passes, can be attributed to their modified microstructure including

intense refinement/even distribution of intermetallic particles, elimination of micropores, and higher bonding quality of the particles/matrix interface which are likely to decrease the initiation probability and retard the propagation of potential subsurface microcracks. However, it is worth noting that the substrate ductilizing seems to encourage the plastic wear in multi-pass FSPed samples which manifest itself as the formation of extruded ridges at the edge of the pins (Figs. 13(b, d, f)). In this mechanism the surface material is displaced without material loss or with insignificant material loss [34].

Figure 14 illustrates the typical friction coefficient graphs of the base, 1P-FSP, and 4P-FSP samples tested at the applied pressures of 0.25 and 0.75 MPa. At the applied pressure of 0.25 MPa, the friction coefficient graph of the base sample shows a growing trend and relatively high fluctuations which can be correlated to the progressive delamination of its tribolayer (Fig. 7(a)) and the abrasions caused by the hard worn out particles entrapped between its tribolayer and the disk (Fig. 9(a)). However, due to the formation of a dense tribolayer on the worn surfaces (Figs. 10(a) and (c)), the FSPed samples exhibit lower average friction coefficients and friction coefficient fluctuation. This is because the formation of tribolayer can decrease the adhesion and reduce the interfacial shear strength [35].

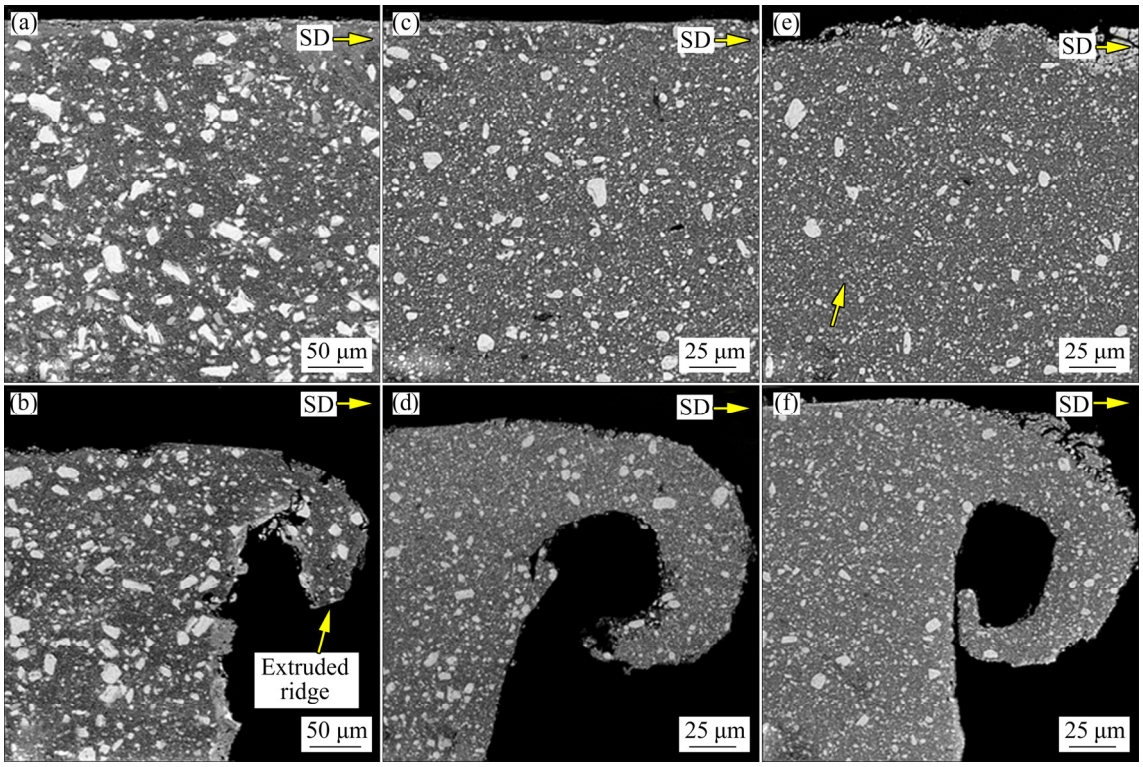

Fig. 13 Worn subsurface microstructures of 1P-FSP (a, b), 2P-FSP (c, d), and 4P-FSP (e, f) samples (applied pressure of 0.75 MPa)

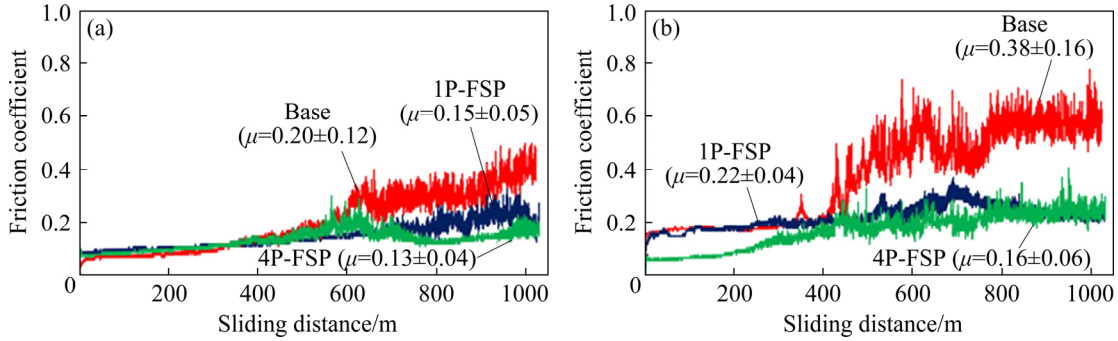

Fig. 14 Variation of friction coefficient of base, 1P-FSP, and 4P-FSP samples against sliding distance at applied pressures of 0.25 MPa (a) and 0.75 MPa (b)

At the higher applied pressures, FSP significantly changes the friction behavior of FVS0812 alloy. According to Fig. 14(b), after a sliding distance of about 400 m, the base sample experiences a sudden increase in its friction coefficient and high friction coefficient fluctuation. The abrupt increase of friction coefficient can be attributed to the severe delamination/microcracking of the substrate and accordingly the instability of the tribolayer. The increased fluctuation of friction coefficient can be also explained by the concurrent effect of the extensive fracture of the intermetallic compounds in the substrate and the abrasions caused by the entrapped intermetallics (two- or three-body abrasive wear) (Figs. 9(b)−(d)). However, the refinement/densification of the microstructure and accordingly better mechanical properties of the substrate increase the tribolayer stability of multi-pass FSPed samples, leading to the lower friction coefficient and friction coefficient fluctuation.

4 Conclusions

(1) FSP effectively refined the coarse θ-$Al_{13}Fe_4$ and α-$Al_{13}(Fe,V)_3Si$ particles present in the microstructure of as-cast FVS0812 alloy, uniformly distributed them within the matrix, and refined its grain structure through dynamic recrystallization. The average size of Fe-rich compounds decreased from about 128 μm in as-cast sample to about 0.4 μm in four-pass FSPed alloy.

(2) FSP also substantially improved the mechanical properties of FVS0812 alloy. For instance, the tensile strength, fracture strain, and microhardness of one- and four-pass FSPed samples were higher than those of the base sample by 1000%, 930%, and 62%, and 1210%, 3340%, and 100%, respectively.

(3) Dispersion-strengthening effect of the intermetallic dispersoids, elimination of the casting defects, formation of a ultrafine-grained structure, work-hardening, and higher bonding quality of the particles/matrix interface are the main factors improving the mechanical properties.

(4) Multi-pass FSP significantly improved the tribological properties of FVS0812 alloy. At the applied pressure of 0.75 MPa, the wear rate and friction coefficient of four-pass FSPed sample decreased by 97% and 52%, respectively. Increasing the substrate resistance against sliding-induced plastic deformation and formation of the stable tribolayers on the surface are likely the most important factors responsible for better tribological properties of FSPed samples.

References

[1] BELOV N A, AKSENOV A A, ESKIN D G. Iron in aluminium alloys: Impurity and alloying element [M]. Milton Park, New York: Taylor and Francis, 2002.

[2] CHEN Zhen-hua, HE Yi-qiang, YAN Hong-ge, HAO Liang, CHEN Zhi-gang, CHAN Gang. Microstructure and mechanical properties of Al−Fe−V−Si/SiC_P composites [J]. Transactions of Nonferrous Metals Society of China, 2007, 17: s238−s243.

[3] SUN S B, ZHENG L J, PENG H, ZHANG H. Microstructure and mechanical properties of Al−Fe−V−Si aluminum alloy produced by electron beam melting [J]. Materials Science and Engineering A, 2016, 659: 207−214.

[4] SUN S B, ZHENG L J, LIU J H, ZHANG H. Selective laser melting of an Al−Fe−V−Si alloy: Microstructural evolution and thermal stability [J]. Journal of Materials Science and Technology, 2017, 33(4): 389−396.

[5] TAN Dun-qiang, LI Wen-xian, XIAO Yu-de, WANG Ri-chu, MA Zheng-qing, XIONG Bai-qing. Phase transition of Al−Fe−V−Si heat-resistant alloy by spray deposition [J]. Transactions of Non-ferrous Metals Society of China, 2003, 13(3): 568−573.

[6] TANG Y P, TAN D Q, LI W X, PAN Z J, LIU L, HU W B. Preparation of Al−Fe−V−Si alloy by spray co-deposition with added its over-sprayed powders [J]. Journal of Alloys and Compounds, 2007, 439(1−2): 103−108.

[7] XIAO Yu-de, WANG Wei, LI Wen-xian. High temperature deformation behavior and mechanism of spray deposited Al−Fe−V−Si alloy [J]. Transactions of Nonferrous Metals Society of China, 2007, 17(6): 1175−1180.

[8] XIAO B L, FAN J, ZHOU L, SHI L. Microstructure and mechanical properties of Al−Fe−V−Si alloy and composites [J]. Journal of Ceramic Processing and Research, 2006, 7(2): 164−166.

[9] ASHRAFI H, ENAYATI M H, EMADI R. Tribological properties of nanostructured Al/$Al_{12}(Fe,V)_3Si$ alloys [J]. Acta Metallurgica Sinica (English Letters), 2014, 28(1): 83−92.

[10] PRŮŠA F, BLÁHOVÁ M, VOJTĚCH D, KUČERA V, BERNATIKOVÁ A, KUBATÍK T, MICHALCOVÁ A. High-strength ultra-fine-grained hypereutectic Al−Si−Fe−X (X=Cr, Mn) alloys prepared by short-term mechanical alloying and spark plasma sintering [J]. Materials, 2016, 9(12): 973.

[11] ZHENG L J, LIU Y Y, SUN S B, ZHANG H. Selective laser melting of Al−8.5Fe−1.3V−1.7Si alloy: Investigation on the resultant microstructure and hardness [J]. Chinese Journal of

Aeronautics, 2015, 20(2): 564−569.

[12] SUN S B, ZHENG L J, LIU Y Y, LIU J H, ZHANG H. Selective laser melting of Al−Fe−V−Si heat-resistant aluminum alloy powder: Modeling and experiments [J]. International Journal of Advanced Manufacturing Technology, 2015, 80(9−12): 1787−1797.

[13] MARSHALL R. Characterization of novel microstructure in Al−Fe−V−Si and Al−Fe−V−Si−Y alloys processed at intermediate cooling rates [D]. Colorado, USA: The Colorado School of Mines, 2015.

[14] BUNK W G J. Aluminium RS metallurgy [J]. Materials Science and Engineering A, 1991, 134: 1087−1097.

[15] LIU Y L, LUO L, SHUN M Z, ZHANG L, ZHAO Y H, WU B L. Microstructure and mechanical properties of Al−5.5Fe−1.1V−0.6Si alloy solidified under near-rapid cooling and with Ce addition [J]. Rare Metals, 2016, 37(12): 1070−1075.

[16] SAHOO K L, DAS S K, MURTY B S. Formation of novel microstructures in conventionally cast Al−Fe−V−Si alloys [J]. Materials Science and Engineering A, 2003, 355(1−2): 193−200.

[17] SAHOO K L, SIVARAMAKRISHNAN C S, CHAKRABARTI A K. Technical note: Modification of cast structure in Al–8.3Fe–0.8V–0.9Si alloy by magnesium treatment [J]. Materials Science and Technology, 2000, 16(2): 227−230.

[18] SAHOO K, KRISHNAN C S, CHAKRABARTI A. Studies on wear characteristics of Al−Fe−V−Si alloys [J]. Wear, 2000, 239(2): 211−218.

[19] SAHOO K L, PATHAK B N. Solidification behaviour, microstructure and mechanical properties of high Fe-containing Al−Si−V alloys [J]. Journal of Materials Processing and Technology, 2009, 209(2): 798−804.

[20] ABBASI M, GIVI M, BAGHERI B. Application of vibration to enhance efficiency of friction stir processing [J]. Transactions of Nonferrous Metals Society of China, 2007, 17(6): 1175−1180.

[21] ABDULMALIK S S, AHMAD R, ASMAEL M B A. The Effect of process parameters in friction stir processing of cast hypereutectic Al–Si alloy [J]. Advanced Science Letters, 2018, 24(6): 3993−3998.

[22] FEKRI SOUSTANI M, TAGHIABADI R, JAFARZADEGAN M, SHAHRIYARI F, RAHMANI A. Improving the tribological properties of Al−7Fe−5Ni alloys via friction stir processing [J]. Journal of Tribology, 2019, 141(12): 1−19.

[23] NOURI Z. Effect of friction stir processing on microstructure, mechanical properties, and tribological behavior of Al−8.5Fe−1.3V−1.7Si alloy [D]. Qazvin, Iran: Imam Khomeini International University, 2018.

[24] TAYLOR R P, MCCLAIN S T, BERRY J T. Uncertainty analysis of metal-casting porosity measurements using Archimedes' principle [J]. International Journal of Cast Metals Research, 1999, 11(4): 247−257.

[25] BECKER H, AMIRKHANYAN L, KORTUS J, LEINEWEBER A. Powder-X-ray diffraction analysis of the crystal structure of the η'-Al_8Fe_3 (η'-$Al_{2.67}Fe$) phase [J]. Journal of Alloys and Compounds, 2017, 721: 691−696.

[26] ZOU Q, ZHAO M, YIN F, LI Z, LIU Y. Phase equilibria in the Al-rich corner of the Al−Fe−Si−V quaternary system at 620 °C [J]. Journal of Phase Equilibria and Diffusion, 2015, 36(3): 274−282.

[27] ANYALEBECHI P N. Analysis of the effects of alloying elements on hydrogen solubility in liquid aluminum alloys [J]. Scripta Metallurgica et Materialia, 1995, 33(8): 1209−1216.

[28] SONG Dong-fu, WANG Shun-cheng, ZHAO Yu-liang, LIU Shu-hong, DU Yong, KANG Yue-hua, WANG Zhi, ZHANG Wei-wen. Effect of melt holding on morphological evolution and sedimentation behavior of iron-rich intermetallic phases in Al−Si−Fe−Mn−Mg alloy [J]. Transactions of Nonferrous Metals Society of China, 2020, 30(1): 1−13.

[29] ARMBRÜSTER M, SCHLÖGL R, GRIN Y. Intermetallic compounds in heterogeneous catalysis — A quickly developing field [J]. Science and Technology of Advanced Materials, 2014, 15(3): 34803.

[30] HERLACH D M, SIMONS D, PICHON P Y. Crystal growth kinetics in undercooled melts of pure Ge, Si and Ge−Si alloys [J]. Philosophical Transactions of The Royal Society A: Mathematical Physical and Engineering Sciences, 2018, 376(2113): 20170205.

[31] MUGICA G W, TOVIO D O, CUYAS J C, GONZÁLEZ A C. Effect of porosity on the tensile properties of low ductility aluminum alloys [J]. Materials Research, 2004, 7(2): 221−229.

[32] ZHANG Z, CHEN D L. Contribution of Orowan strengthening effect in particulate-reinforced metal matrix nanocomposites [J]. Materials Science and Engineering A, 2008, 483–484: 148–152.

[33] SHARMA V, PRAKASH U, KUMAR B V M. Surface composites by friction stir processing: A review [J]. Journal of Materials Processing and Technology, 2015, 224: 117−134.

[34] VERRET R, RIDGE I. Wire rope forensics—CASAR special wire ropes [M]. Aachen, Germany: PR GmbH, 2005.

[35] NADIM A, TAGHIABADI R, RAZAGHIAN A. Effect of Fe-impurity on tribological properties of Al−15Mg_2Si composite [J]. Transactions of Nonferrous Metals Society of China, 2018, 28(6): 1084−1093.

多道次搅拌摩擦加工改善传统铸造 Al−8.5Fe−1.3V−1.7Si 合金的摩擦学性能

Z. NOURI, R. TAGHIABADI

Department of Materials Science and Metallurgy, Imam Khomeini International University, Qazvin, Iran

摘　要：研究多道次搅拌摩擦加工(FSP)对传统铸造 Al−8.5Fe−1.3V−1.7Si (FVS0812)合金摩擦学性能的影响。分别在 0.25、0.50、和 0.75 MPa 的载荷下，于室温下进行销−盘式干滑动磨损实验。结果表明，FSP 大幅细化合金显微组织中粗大的 θ-$Al_{13}Fe_4$ 片状晶和 α-$Al_{12}(Fe,V)_3Si$ 金属间化合物，改善其分布，并消除金属间化合物相关的缺陷，从而提高合金的力学性能，特别是其延展性，进而提高在其磨损表面形成的摩擦保护层的稳定性。磨损实验结果表明，经 FSP 的复合材料其摩擦学性能得到改善，尤其是在较高的外加载荷下。例如，当载荷为 0.75 MPa 时，与铸态样品相比，经四道次 FSP 的样品其磨损率和平均摩擦因数分别降低 97%和 52%。磨损表面和磨屑的扫描电镜分析表明，铸态样品的磨损机制为摩擦层严重的剥层/磨粒磨损和微裂纹，FSP 态样品的磨损机制为轻度的剥层/磨粒磨损和轻微的塑性磨损。

关键词：搅拌摩擦加工；Al−8.5Fe−1.3V−1.7Si (FVS0812)合金；金属间化合物；摩擦学

(Edited by Xiang-qun LI)